9-21-2011

Using Sterics to Promote Reactivity in *fac*-Re(CO)$_3$ Complexes of Some 'Non-Innocent' NNN-Pincer Ligands

Sarath Wanniarachchi
Marquette University, sarath.wanniarachchi@marquette.edu

Brendan J Liddle
Marquette University

John Toussaint
Marquette University

Sergey Lindeman
Marquette University, sergey.lindeman@marquette.edu

Brian Bennett
Marquette University, brian.bennett@marquette.edu

See next page for additional authors

Accepted version. *Dalton Transactions*, Vol. 40, No. 35 (September 21, 2011): 8776-8787. DOI.
Brian Bennett was affiliated with the Medical College of Wisconsin at the time of publication.

Using Sterics to Promote Reactivity in *fac*-Re(CO)3 Complexes of Some 'Non-Innocent' NNN-Pincer Ligands

Sarath Wanniarachchi
Department of Chemistry, Marquette University
Milwaukee, WI
Brendan J. Liddle
Department of Chemistry, Marquette University
Milwaukee, WI
John Toussaint
Department of Chemistry, Marquette University
Milwaukee, WI
Sergey V. Lindeman
Department of Chemistry, Marquette University
Milwaukee, WI
Brian Bennett
Department of Biophysics, Medical College of Wisconsin
Milwaukee, WI
James R. Gardinier
Department of Chemistry, Marquette University
Milwaukee, WI

Abstract: Two new redox active ligands based on di(2-(3-organopyrazolyl)-ptolyl)amine have been prepared in order to investigate potential effects of steric bulk on the structures, electronic properties, or reactivity of tricarbonylrhenium(I) complexes. Replacing the hydrogens at the 3-pyrazolyl

Dalton Transactions, Vol. 40, No. 35 (September 2011): pg. 8776-8787. DOI.

positions with alkyl groups causes significant distortion to the ligand framework due to potential interactions between these groups when bound to a *fac*-$Re(CO)_3$ moiety. The distortions effectively increase the nucleophilic character of the central amino nitrogen and ligand-centered reactivity of the metal complexes.

Introduction

Metal complexes of pincer ligands are receiving increased attention for studies in a wide range of topical areas from catalysis to bioinorganic and materials chemistry.[1] The appeal of these complexes arises from their generally high stability and the unusual reactivity that suitably designed ligands can impart on a metal center. Further interest is educed by emergent reports documenting non-innocent pincer variants that promote unexpected chemistry.[2] We recently introduced a new non-innocent NNN-pincer ligand based on di(2-(pyrazolyl)-*p*-tolyl)amine and its various tricarbonylrhenium(I) complexes (Fig. 1).[3]

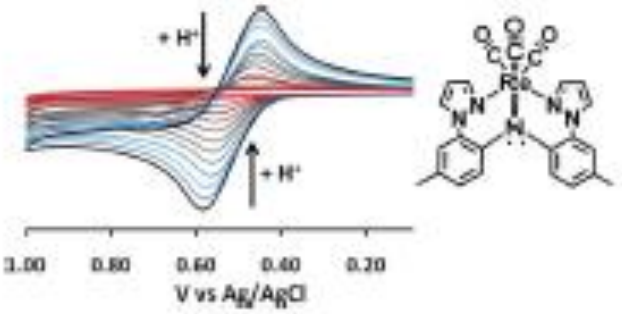

Fig. 1 Electrochemical response of a tricarbonylrhenium(I) NNN-pincer complex in CH_2Cl_2 to HBF_4.

The quasi-reversible electrochemistry associated with the (metal-bound) ligand oxidation could be reproducibly turned 'off' or 'on' by protonation and deprotonation reactions with Brønsted acids or bases, respectively. Moreover, the one-electron oxidized product $[Re(CO)_3(\mathbf{L^H})]^+$ was demonstrated to contain a ligand-centred radical by IR and EPR experiments. These results were also suggested by a theoretical (DFT) study that showed that most of the spin density was located on the central amido nitrogen, substantial contributions were found at the ortho- and para- aryl carbons, and a smaller contribution extended onto a metal d-orbital. During the course of that work it

Dalton Transactions, Vol. 40, No. 35 (September 2011): pg. 8776-8787. DOI.

occurred to us that if the stability of the ligand cation radical results from hole delocalization over the entire π-conjugated diarylamine framework, it should be possible to alter the stability (i.e. increase the reactivity) of this cation or even its precursors by increasing the aryl-aryl dihedral angle, effectively disrupting conjugation. Inspection of the structures of $Re(CO)_3(\mathbf{L^H})$ and associated derivatives suggested that this goal could be achieved simply by placing steric bulk at the 3-position of the pyrazolyls. Herein we fully document the successful, yet surprising, results of these efforts including the preparation of two new NNN-pincer ligands (R = Me, iPr, Scheme 1) and the properties of their various $Re(CO)_3$ complexes.

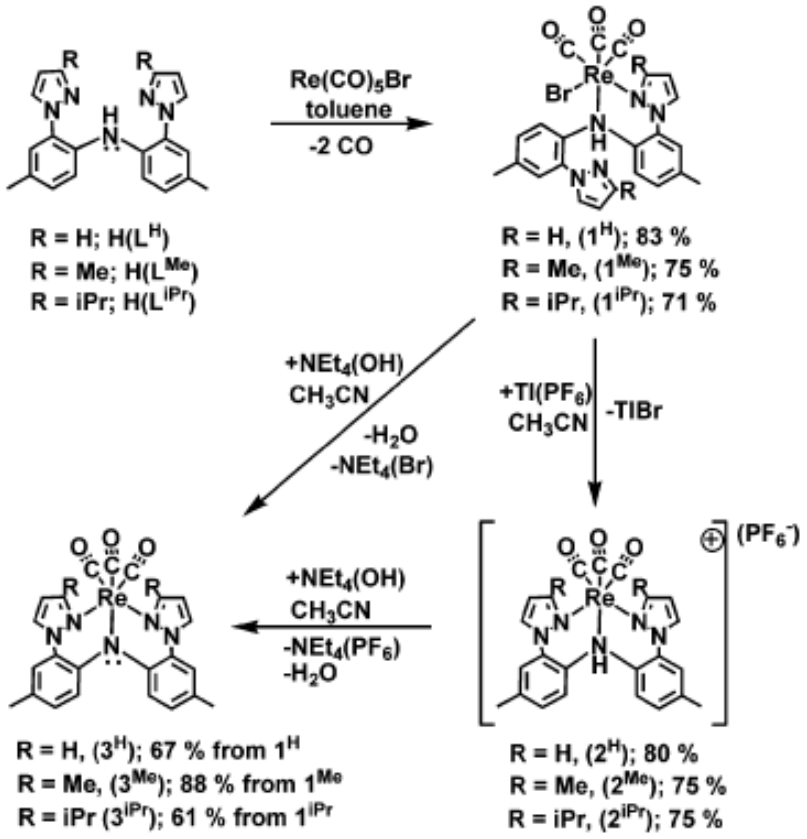

Scheme 1 Summary of preparative routes to the various $Re(CO)_3$ complexes of the NNN-pincer ligands used in this work.

Dalton Transactions, Vol. 40, No. 35 (September 2011): pg. 8776-8787. DOI.

Results and Discussion

Preparation

The syntheses of the ligands and *fac*-$Re(CO)_3$ complexes follows methodology similar to that reported for di(2-(pyrazolyl)-ptolyl) amine, H(**L^{H}**) and its complexes.[3] The preparative routes to the complexes are summarized in Scheme 1. For the ligand syntheses described in the experimental, the CuI-catalyzed amination reactions4 between $HN(2\text{-Br-p-tolyl})_2$[5] and either 3-methyl- or 3-isopropyl-pyrazole[6] proceeded smoothly to give 60–65% yields of H(**L^{Me}**) or H(**L^{iPr}**) simply by heating neat mixtures for 1 d at 200°C followed by conventional workup. In contrast, low yields of H(**L^{H}**) are obtained when heating neat reaction mixtures because unsubstituted pyrazole distills out of the reaction mixture and condenses as a solid onto cooler parts of the reaction apparatus; here, the addition of minimal xylenes helps to wash pyrazole back to the heterogeneous reaction mixture. The longer reaction time required for the preparation of H(**L^{H}**) (2d, monitored by TLC, 69% isolated yield) is likely limited by the distillation temperature of xylenes (bp = 151°C). For the 3-organopyrazolyl derivatives, only the desired isomer of H(**L^{Me}**) or H(**L^{iPr}**) as depicted in the top left of Scheme 1 was obtained (from NMR spectral data and crystallographic determinations of the free ligand, H(**L^{Me}**)† and of all metal complexes with these ligands). Hypothetical di(2-(5-R-pyrazolyl)-*p*-tolyl)amine isomers (with both R groups situated proximal rather than distal to the aryls) or mixed 3,5-isomers have not been detected. In the IR spectrum (KBr) of each ligand, the N–H stretching frequency occur as a medium intensity, sharp bands at rather low energy for 2° arylamines (3261 cm^{-1} for H(**L^{H}**); 3297 cm-1 for H(**L^{Me}**); 3296 cm^{-1} for H(**L^{iPr}**)) which typically occur nearer to 3400 cm^{-1}, presumably a result of the intramolecular hydrogen bonding.[7]

The reactions between the free ligands [of general notation H(**L^{R}**)] and $Re(CO)_5Br$ in boiling toluene causes elimination of two equivalents of CO concomitant with the precipitation of the *fac*-$ReBr(CO)_3$[H(**L^{R}**)] complexes (1^{R}) as analytically pure colorless powders. The ensuing reactions of **1^{R}** with $TlPF_6$ in CH_3CN provide {fac-$Re(CO)_3$[H(**L^{R}**)]}(PF6) (**2^{R}**). As found in related diarylamine systems,[8] complexation of the ligands to metal centers causes a progressive red-shift in the N–H stretching frequency with increasing

Dalton Transactions, Vol. 40, No. 35 (September 2011): pg. 8776-8787. DOI.

electron density of the metal center. For instance, ν_{NH} = 3243 cm^{-1} for **2^{H}** and ν_{NH} = 3147 cm^{-1} for **1^{H}**. Finally, the reactions of colorless **1^{R}** or **2^{R}** in CH_3CN with the Brønsted base $(NEt_4)(OH)$ leads immediately to the formation of the corresponding yellow *fac*-$Re(CO)_3$(**L^{R}**) complexes (**3^{R}**) where the hydrogen on the diarylamine has been eliminated (after reaction with hydroxide to give H_2O). Of the two routes to **3^{R}**, that starting from **1^{R}** is preferred since one less synthetic step is required (and in our hands it was easier to separate **3^{R}** from NEt_4Br than from $NEt_4(PF_6)$). In either case, it is noted that the reaction time is best kept short (15 min) as longer reaction times give lower yields due to a slow but competing decomposition reaction that produces increasing amount of 'free' ligand H(**L^{R}**); the nature of the rhenium-containing decomposition by-product is unclear. Fortuitously, the separation of **3^{R}** and other products is facilitated by the significantly different solubilities of the desired and unwanted products in MeOH or in benzene and Et_2O.

Solid State Structures

`The structures of H(**L^{Me}**) and the six rhenium complexes 1^{R}, 2^{R}, and 3^{R} (R = Me, iPr) were determined by single crystal X-ray diffraction; those of H(**L^{H}**), 1^{H}, 2^{H}, and 3^{H} were reportedpreviously. Representative structures for **1^{Me}**, **2^{Me}**, and **3^{Me}** are provided in Fig. 2–4 while other new structures are provided in the Electronic Supplementary Information (ESI).† Selected interatomic distances and angles are listed in Table 1.

Table 1 Selected bond distances and interatomic angles for **1^{R}**, **2^{R}**, and **3^{R}** (R = H, Me, iPr)

Distance (Å)	**1^{H}**	**1^{Me}**	**1^{iPr}**	**2^{H}**	**2^{Me}**	**2^{iPr}**	**3^{H}**	**3^{Me}**	**3^{iPr}**	**4^{iPr}**
Re–Br	2.6193(8)	2.6312(3)	2.6123(3)	—	—	—	—	—	—	—
Re–N1	2.265(6)	2.268(2)	2.263(3)	2.257(4)	2.251(2)	2.265(2)	2.163(2)	2.178(3)	2.183(2)	2.306(1)
Re–N11	2.182(6)	2.198(2)	2.198(2)	2.174(3)	2.175(2)	2.187(2)	2.173(2)	2.191(3)	2.198(2)	2.177(1)
Re–N21	—	—	—	2.180(3)	2.181(2)	2.205(2)	2.148(2)	2.207(3)	2.219(2)	2.185(1)
Re–C41	1.899(8)	1.915(3)	1.932(3)	1.916(5)	1.923(3)	1.921(3)	1.914(3)	1.919(3)	1.923(2)	1.905(2)
Re–C42	1.928(8)	1.922(3)	1.934(3)	1.944(5)	1.927(3)	1.937(3)	1.923(3)	1.921(4)	1.922(2)	1.922(2)
Re–C43	1.946(8)	1.932(3)	1.947(4)	1.933(5)	1.929(3)	1.925(3)	1.948(3)	1.909(3)	1.915((2)	1.925(2)
C41–O1	1.165(9)	1.147(3)	1.132(4)	1.149(5)	1.141(4)	1.144(4)	1.158(3)	1.154(4)	1.150(3)	1.153(2)
C42–O2	1.143(10)	1.147(3)	1.136(4)	1.129(5)	1.148(4)	1.140(4)	1.147(3)	1.155(5)	1.151(3)	1.153(2)
C43–O3	1.091(9)	1.113(3)	1.050(4)	1.140(5)	1.148(4)	1.141(4)	1.138(3)	1.153(4)	1.152(3)	1.146(2)
N1H1···N21	1.913(9)	2.03(3)	2.13(4)	—	—	—	—	—	—	—
⊥N1···(C_2Re)[a]	0.383(8)	0.396(2)	0.385(3)	0.492(5)	0.515(3)	0.519(3)	0.191(2)	0.431(3)	0.426(2)	0.576(2)
Angles/torsions (°)										
N1–Re–N11	77.2(2)	77.91(8)	77.61(9)	77.72(13)	77.03(9)	76.30(9)	79.26(8)	76.59(10)	75.27(7)	78.25(5)
N1–Re–N21	—	—	—	83.68(13)	83.45(8)	83.57(8)	81.57(8)	84.27(11)	85.09(7)	83.30(5)
Fold (N11)[b]	138.8(5)	136.4(2)	135.1(2)	130.6(5)	127.0(4)	125.2(2)	136.2(2)	127.2(3)	125.5(2)	121.0(2)
Fold (N21)[c]	—	—	—	159.2(4)	152.6(4)	153.2(2)	147.4(2)	164.1(3)	161.9(2)	144.2(2)
ReN11–N12C2	−16.1(9)	−12.8(3)	12.0(4)	14.0(5)	5.1(3)	−1.9(3)	−14.3(3)	−1.3(4)	6.4(3)	−11.6(2)
ReN21–N22C32	—	—	—	−9.8(6)	0.4(4)	15.9(3)	8.3(3)	−36.(4)	−33.0(3)	1.5(2)
pz(N11)–tol(C1)	40.8(6)	39.8(3)	40.7(2)	43.6(5)	38.5(3)	37.3(2)	45.0(2)	38.5(2)	35.7(1)	50.9(1)
pz(N21)–tol(C31)	13.6(6)	23.7(3)	28.6(2)	27.2(5)	29.8(3)	37.2(2)	36.3(2)	37.9(2)	38.6(1)	28.9(1)
tol(C1)–tol(C31)	76.9(6)	66.7(3)	67.5(2)	74.6(4)	71.5(3)	69.7(2)	28.4(2)	78.8(2)	77.9(1)	72.9(1)
Σ∠'s about N1[d]	344.4(7)	343.2(3)	344.2(3)	334.5(4)	332.0(2)	331.7(2)	355.6(2)	338.6(3)	339.2(2)	326.1(2)

pz = mean plane of pyrazolyl ring, tol = mean plane of C6 ring of tolyl group;[a] Distance of normal vector between N1 and mean plane of atoms Re, C1, and C31; [b] fold angle between Re and the centroids (Ct) of N1 and N11 and Ct of C1 and N12; [c] fold angle between Re and the centroids (Ct) of N1 and N21 and Ct of C31 and N22; [d] involving Re, C1, and C31.

Dalton Transactions, Vol. 40, No. 35 (September 2011): pg. 8776-8787. DOI.

All of the rhenium complexes retain the *fac*-$Re(CO)_3$ moiety and all are chiral (with C_1-symmetry) as a result of the various ligand conformations (*vide infra*).

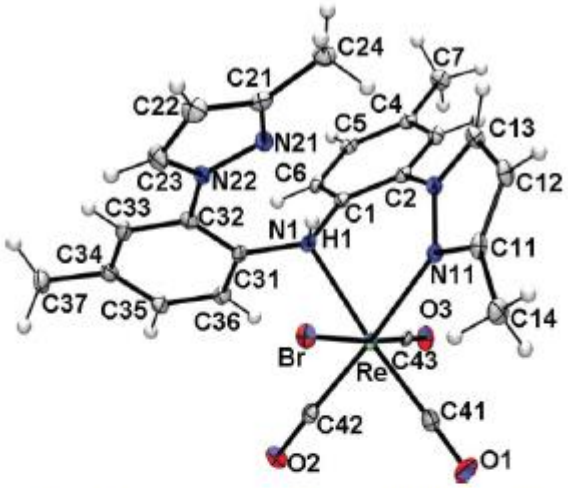

Fig. 2 Structure of *fac*-$ReBr(CO)_3[H(L^{Me})]$, $\mathbf{1}^{Me}$.

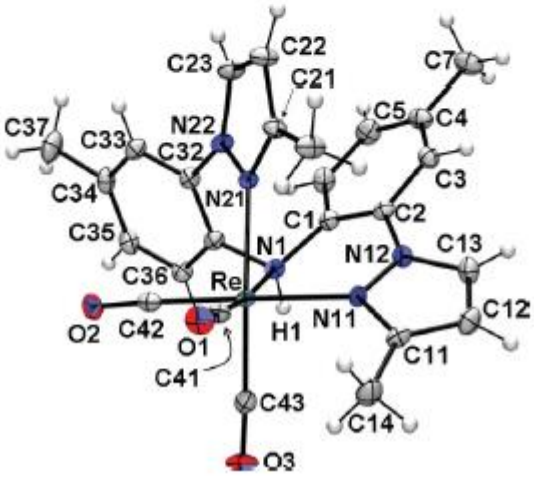

Fig. 3 Structure of the cation in $\{fac\text{-}Re(CO)_3[H(L^{Me})]\}(PF_6)$, $\mathbf{2}^{Me}$.

For the $\mathbf{1}^{R}$ series, the ligand is bound to the metal in a chelating k^2N-manner *via* the central amino nitrogen and one pyrazolyl nitrogen. In each of these cases, the amino hydrogen is oriented toward the axial bromide rather than the axial carbonyl. For each, the rhenium-nitrogen bond involving the amino group (Re–N1, or $Re–N_{Ar}$, *ca*. 2.27 Å) is longer than that involving the pyrazolyl (Re–N11, or $Re–N_{pz}$, *ca*. 2.19 Å).

Dalton Transactions, Vol. 40, No. 35 (September 2011): pg. 8776-8787. DOI.

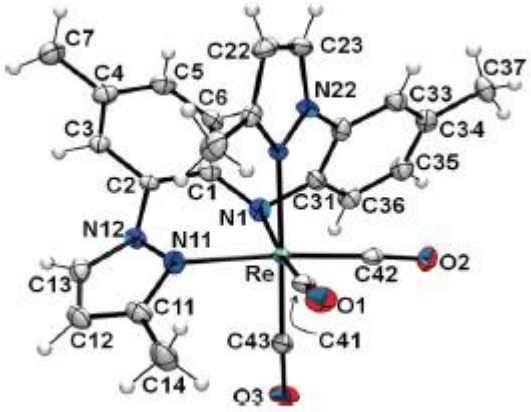

Fig. 4 Structure of *fac*-$Re(CO)_3(L^{Me})$, 3^{Me}.

The bond distances in this series of complexes are typical of other N,N-chelating ligands containing the fac-$Re(CO)_3Br$ moiety such as in the closely related $Re(CO)_3Br[H(pzAn^{Me})]$ ($H(pzAn^{Me})$ is 2-pyrazolyl-4-toluidine; Re–Br = 2.628 Å , $Re–N_{Ar}$ = 2.219 Å , and $Re–N_{pz}$ 2.179 Å)9 or those in the NNN-pincer- relative, $ReBr(CO)_3$[bis(1-methyl-1*H*-benzoimidazol-2-ylmethyl)amine)] (Re–Br, $Re–N_{avg}$ = 2.23–2.28 Å).[10] Within the series $\mathbf{1^R}$, the steric profile of the 3-R-pyrazolyl substituent has the expected but small effect on $Re–N_{pz}$ bond distances with the unsubstituted derivative having a shorter bond (2.18 Å) than the 3-substituted derivatives (ca. 2.20 Å) but there is no significant difference in the Re–N1 (amino nitrogen) bond distances (*ca*. 2.26 Å). Interestingly, the most striking influence of 3-pyrazolyl substitution occurs with the interatomic distances and angles associated with the 'free' arm of the ligand. For $\mathbf{1^H}$, there is a relatively short hydrogen bonding interaction between the amino hydrogen H1 and the free pyrazolyl nitrogen N21 (N1H1…N21: 1.91 Å , 140°) that brings the 'free' pyrazolyl and tolyl groups closer to coplanarity (dihedral between mean planes of 14°) than those rings that are bound to rhenium (dihedral between mean planes of 41°). For $\mathbf{1^{Me}}$ and $\mathbf{1^{iPr}}$, the hydrogen bonding interaction becomes progressively longer (and presumably weaker) and the pz-tolyl dihedral becomes larger with increasing steric bulk (N1H1…N21: 2.02 Å, 141°and pztolyl dihedral 24° for $\mathbf{1^{Me}}$ and N1H1…N21: 2.13 Å , 153° and pz-tolyl dihedral 29° for $\mathbf{1^{iPr}}$). A similar observation is made for the structures of the free ligands [two independent molecules: avg. N1H1…N21: 2.04 Å, 132° and pz-tolyl

Dalton Transactions, Vol. 40, No. 35 (September 2011): pg. 8776-8787. DOI.

dihedral 30° for H(LH); N1H1…N21: 2.20Å, 129° and pz-tolyl dihedral 43° for H(LMe)].

For each ionic derivative 2R, the ligand binds rhenium in a κ^3N-manner giving a *fac*-ReN_3C_3 kernel. The average Re–N distances in $\mathbf{2^R}$ are shorter than the corresponding distances in $\mathbf{1^R}$, as expected from the cationic nature of the former. Within the series of $\mathbf{2^R}$, 3-pyrazolyl substitution results in gradual increase in Re–N_{pz} distances with increasing steric bulk but, as with $\mathbf{1^R}$, substitution has little impact on the Re–N1 distances. In $\mathbf{2^R}$, there are two six-memberReN_3C_2 chelate rings that can be differentiated by small differences in Re–N_{pz} bond lengths, chelate bite and fold angles. As found in Table 1, one chelate ring (containing N11) has a shorter Re–N_{pz} bond, a smaller chelate bite (N1ReN11 angle) and a greater chelate ring puckering (more acute fold angle) than the other chelate ring containing N21. The chelate ring with smaller bite and fold angles in $\mathbf{2^R}$ has similar metrical parameters to those found in $\mathbf{1^R}$. A final small but noteworthy effect of changing 3-pyrazolyl substituents is found by examining the local coordination geometry around the amino nitrogen N1. The 3-organopyrazolyl groups in $\mathbf{2^{Me}}$ and $\mathbf{2^{iPr}}$ enforce greater pyramidalization about N1 (relative to the mean plane defined by C1 C31 and Re) compared to the unsubstituted pyrazolyl derivative $\mathbf{2^H}$. That is, the sum of angles about N1 (Σ∠'s about N1, not involving N1–H1) and the perpendicular distance between N1 and the mean plane defined by C1 C31 and Re, ⊥N1…(C_2Re), are 332° and 0.52 Å for $\mathbf{2^{Me}}$ and $\mathbf{2i^{Pr}}$ but are 334° and 0.49 Å for $\mathbf{2^H}$; a planar nitrogen would have ideal values of 360 ° and 0Å .

In a manner similar to $\mathbf{2^R}$, the ligands in $\mathbf{3^R}$ bind rhenium in a k^3N-manner giving *fac*-ReN_3C_3 kernels. Deprotonation of the amino hydrogen is accompanied by a significant shortening of the Re–N_{Ar} bond in $\mathbf{3^R}$ (*ca*. 2.19 Å) relative to the corresponding distances in $\mathbf{1^R}$ (*ca*. 2.27 Å) or $\mathbf{2^R}$ (*ca*. 2.26 Å). Within the series $\mathbf{3^R}$, the Re–N_{Ar} bond is longer for derivatives with 3-organo substituents (2.163(2) Å for $\mathbf{3^H}$, 2.178(3) Å for $\mathbf{3^{Me}}$ and 2.183(2)Å for $\mathbf{3^{iPr}}$). As highlighted in Fig. 5, the structure of $\mathbf{3^H}$ is distinct from those of $\mathbf{3^{Me}}$ and $\mathbf{3^{iPr}}$ in that the former approaches mirror symmetry (disregarding the tolyl-tolyl dihedral and slight differences in chelate ring distortions that give the complex actual C_1 symmetry) with a short average Re–N_{pz} distance (2.16 Å) and a nearly planar amido nitrogen (Σ∠'s about N1 = 356°). In

Dalton Transactions, Vol. 40, No. 35 (September 2011): pg. 8776-8787. DOI.

contrast, the latter two complexes more closely resemble their protonated counterparts $\mathbf{2^{Me}}$ and $\mathbf{2^{iPr}}$ each with decidedly C_1 symmetry. Relative to $\mathbf{3^{H}}$, $\mathbf{3^{Me}}$ and $\mathbf{3^{iPr}}$ have longer Re–N_{pz} bond distances (2.20Å for $\mathbf{3^{Me}}$ and 2.21 v for $\mathbf{3^{iPr}}$) and more pyramidal amido nitrogens (Σ∠'s about N1 = 339° for each). Presumably, potential steric interactions involving 3-organopyrazolyl groups enforce the observed C_1 symmetric conformations, and make hypothetical pseudo-Cs symmetric conformations of either $\mathbf{3^{Me}}$ or $\mathbf{3^{iPr}}$ much higher energy.

Fig. 5 Overlay of structures for $\mathbf{3^R}$ (R = H, black thin wireframe; R = Me, red capped stick; R = iPr, green capped stick) referenced to common $N_{pz}Re(CO)_3$ cores.

Solution Characterization

Selected electrochemical and IR spectral data for complexes $\mathbf{1^R}$–$\mathbf{3^R}$(R = H, Me, iPr) are given in Table 2. The current discussion of solution properties will center on the data for $\mathbf{3^R}$ because of their interesting electronic properties and disparate reactivity patterns is the focus of this work. The solution characterization data of analytically pure $\mathbf{1^R}$–$\mathbf{3^R}$ (R = H, Me, iPr) are less germane to the central point of the work but are noteworthy since they are unexpectedly complex, as described previously for R = H.[3] That is, NMR and other solution data show that all $\mathbf{1^R}$ are involved in ionization equilibria to form $\mathbf{2^R}$ and another ionic intermediate, presumably five-coordinate [$Re(CO)_3(\varkappa^2$-H$\mathbf{L^R}$)+](Br−)†. All $\mathbf{2^R}$ and ionized forms of $\mathbf{1^R}$ are also involved in dynamic exchange processes. Full details of the complex NMR data for these complexes can be found in the ESI.†

Dalton Transactions, Vol. 40, No. 35 (September 2011): pg. 8776-8787. DOI.

Table 2 IR and electrochemical data for various $Re(CO)_3$ complexes

Compound	ν_{C-O} (cm^{-1})[a]	$E_{1/2}$ (V *vs.* Fc/Fc^+)[a,b]
$\mathbf{1}^{H}$	2029, 1921, 1898; avg 1949[c]	*irr.* E_{pa} = +1.07, +0.67, +0.23
$\mathbf{1}^{Me}$	2027, 1920, 1896; avg. 1948[c]	*irr.* E_{pa} = +1.04, +0.75, +0.25
$\mathbf{1}^{iPr}$	2027, 1919, 1894; avg. 1947[c]	*irr.* E_{pa} = +1.04, +0.75, +0.20
$\mathbf{2}^{H}$	2040, 1950, 1930; avg. 1973	*irr.* E_{pa} = +1.17
$\mathbf{2}^{Me}$	2040, 1935, 1919; avg 1965	*irr.* E_{pa} = +1.27
$\mathbf{2}^{iPr}$	2038, 1936, 1921; avg 1965	*irr.* E_{pa} = +1.25
$\mathbf{3}^{H}$	2013, 1901, 1876; avg. 1930	+0.001
$\mathbf{3}^{Me}$	2009, 1903, 1879; avg. 1930	−0.011
$\mathbf{3}^{iPr}$	2008, 1898, 1876; avg. 1927	−0.015
$(\mathbf{3}^{H})^+$	2034, 1927; avg. 1963	—
$(\mathbf{3}^{Me})^+$	2038, 1931; avg. 1967	—
$(\mathbf{3}^{iPr})^+$	2038, 1933; avg. 1968	—
$\mathbf{4}^{Me}$	2036, 1930, 1923; avg. 1963	not measured
$\mathbf{4}^{iPr}$	2033, 1927, 1915; avg. 1958	not measured

[a] CH_2Cl_2 solution; [b] CH_2Cl_2, 100 mV s^{-1}, TBAH; [c] major species, see ESI† for more details.

The NMR spectra for $\mathbf{3}^{R}$ are simpler than expected based on the low-symmetry solid state structures owing to rapid processes that interchange supposedly symmetrically inequivalent halves of the ligands (or that invert conformations of chelate rings). That is, if the solid state structures were retained, two sets of resonances for pyrazolyl and tolyl hydrogens would be expected but only one set is observed (*vide infra*). In surprising contrast to $\mathbf{1}^{R}$, $\mathbf{2}^{R}$ or $\mathbf{4}^{R}$, the rate of the exchange process in $\mathbf{3}^{R}$ could not be slowed down enough to be measured by NMR even when CD_2Cl_2 or acetone-d_6 solutions are cooled to 193 K. Given that the exchange processes can be frozen at low temperatures for derivatives with quaternary amino nitrogens ($\mathbf{1}^{R}$, $\mathbf{2}^{R}$ or $\mathbf{4}^{R}$, *vide infra*),† nitrogen inversion facilitates the exchange processes of $\mathbf{3}^{R}$.

In either the solid state or solution, the IR spectrum of each $\mathbf{3}^{R}$ gives a characteristic pattern of three C–O stretching bands (Table 1) for *fac*-$Re(CO)_3$ units; the N–H stretching band is also absent. In accord with expectations based on the increasing electron density at metal centres (and greater back-bonding), the CO stretches appear at lower energy relative to $\mathbf{1}^{R}$ and $\mathbf{2}^{R}$ where average stretching frequencies decrease in the order $\mathbf{2}^{R} > \mathbf{1}^{R} > \mathbf{3}^{R}$. For $\mathbf{3}^{R}$, replacement of 3-pyrazolyl hydrogens for more electron donating methyl or isopropyl substituents has a surprisingly small electronic effect, as

Dalton Transactions, Vol. 40, No. 35 (September 2011): pg. 8776-8787. DOI.

indicated by the nearly identical average CO stretching frequencies. It is likely that any potential inductive electronic effects may be offset by steric interactions that enforce longer Re–N bonds along the series **3^{H}** < **3^{Me}** < **3^{iPr}**.

The electrochemistry of each **3^{R}** is distinct from their counterparts **1^{R}** or **2^{R}** (Table 1) as each **3^{R}** in CH_2Cl_2 shows a quasi-reversible oxidation near Br versus Fc/Fc^+ (Fig. 6, i_{pc}/i_{pa} = 1, but $\Delta E = E_{pa} - E_{pc}$ increases as a function of scan rate); **1^{R}** and **2^{R}** have irreversible oxidations ($i_{pc}/i \ll 1$ and $\Delta E \gg 59$ mV) at higher potentials. The oxidation potentials of **3^{Me}** and **3^{iPr}** are nearly equivalent and are only slightly (10–15mV) more favourable than that of 3H. Interestingly, in CH_3CN the oxidation becomes reversible for **3^{H}** and **3^{Me}** but not for **3^{iPr}**.† Spectrophotometric titrations with organic oxidants indicate that the oxidation is a one-electron event, as discussed later.

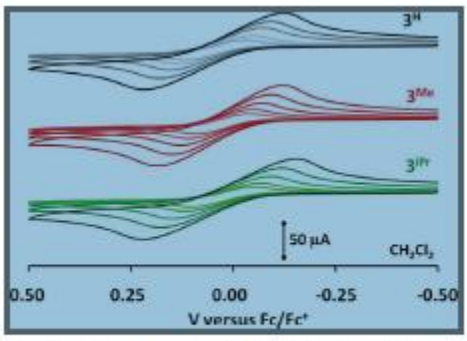

Fig. 6 Cyclic voltammograms of *fac*-$Re(CO)_3(L^R)$ (3^R) complexes in CH_2Cl_2 each taken with scan rates of 50 (inner), 100, 200, 400, and 800 (outer) mV s^{-1}.

Dalton Transactions, Vol. 40, No. 35 (September 2011): pg. 8776-8787. DOI.

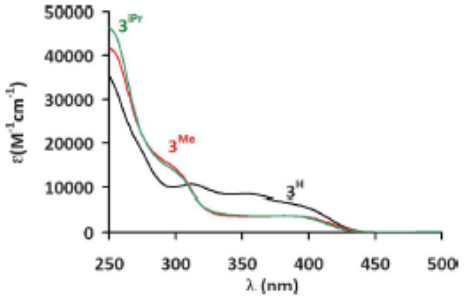

Fig. 7 Overlay of electronic absorption spectra for $\mathbf{3^R}$ in CH_2Cl_2 (R = H, black; R = Me, red; R = iPr, green).

The electronic absorption spectra of $\mathbf{3^R}$ complexes in CH_2Cl_2 are found in Fig. 7. The spectra are qualitatively similar, as might be expected, but there are subtle differences that distinguish the R = H from the R = Me, iPr derivatives. Each spectrum has two bands above about 350 nm that give rise to the yellow colour of the complexes. For $\mathbf{3^H}$ these low energy bands are more intense ($\varepsilon \sim 8000–10000$ $M^{-1}cm^{-1}$) than those of either $\mathbf{3^{Me}}$ or $\mathbf{3^{iPr}}$ ($\varepsilon \sim 5000$ $M^{-1}cm^{-1}$). For $\mathbf{3^H}$ the lowest energy band (400 nm, $\varepsilon \sim 8000$ M-1cm-1) is less intense than the second lowest energy band (360 nm, $\varepsilon \sim 10000$ M-1cm-1) while the opposite is true for either $\mathbf{3^{Me}}$ or $\mathbf{3^{iPr}}$; for the latter deconvolution is necessary to observe the second lowest energy band.

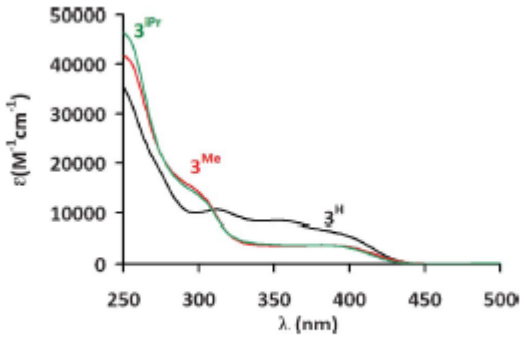

Fig. 7 Overlay of electronic absorption spectra for $\mathbf{3^R}$ in CH_2Cl_2 (R = H, black; R = Me, red; R = iPr, green).

Since these two bands are absent in $\mathbf{1^R}$ and $\mathbf{2^R}$, they are attributed to transitions between electronic states involving an engaged $d\pi–p\pi$ interaction (between the metal and available lone pair on the central amido nitrogen of the ligand). Such an assessment was bolstered by theoretical calculations (TD-DFT, see ESI for full details)

Dalton Transactions, Vol. 40, No. 35 (September 2011): pg. 8776-8787. DOI.

where the lowest energy band enveloped transitions between the HOMO and various LUMO(+N) (N = 0–4) levels and the second-lowest energy band involves transitions between the HOMO(-1) and the various LUMO(+N) (N = 0–4) levels. As illustrated in Fig. 8, the HOMO is mainly a π-based orbital centralized on the pincer ligand but extends onto a d-orbital of rhenium. The HOMO(-1) is qualitatively similar to the HOMO but with greater rhenium character. For **3^{H}**, conjugation across both 2-pyrazolyl-*p*-tolyl 'arms' of the pincer ligand is evident from the atomic orbital contributions to the HOMO and to a lesser extent the HOMO(-1) but for **3^{Me}** and **3^{iPr}** the conjugation appears confined to only one 'arm' of the ligand.

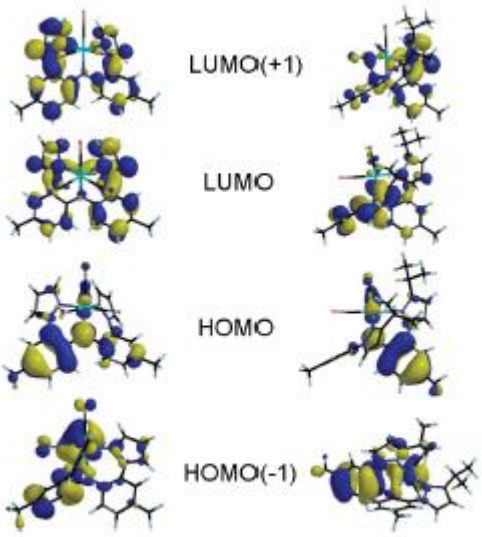

Fig. 8 Comparison between frontier orbitals of 3^{H} (left) and 3^{iPr} (right) from theoretical calculations (B3LYP/LACVP).

The LUMO and LUMO(+1) are mainly π*-orbitals of the pincer ligand while next three higher-energy virtual orbitals are those of the tricarbonyl fragment. As such these two lowest energy bands can be considered to have metal–ligand-to-ligand charge transfer (MLLCT) character in accord with conventions used elesewhere.[11] The higher energy band found at 300 nm is likely due to charge transfer transitions involving the tricarbonylrhenium fragment as found in related systems[7] while the high-intensity bands found below 275 nm are likely π–π* transitions on the basis of energy and intensity considerations.

Dalton Transactions, Vol. 40, No. 35 (September 2011): pg. 8776-8787. DOI.

Reactivity

Given the availability of a lone pair of electrons on the central nitrogen in $\mathbf{3^R}$, the potential for these complexes to engage in nucleophilic substitution (S_N2) reactions[12] as in Scheme 2 was evaluated. Initial stoichiometric NMR experiments performed in C_6D_6 at room temperature showed either no or trace reaction after a couple of hours. However, in hot (45°C) acetone and with a 10-fold excess of MeI, complexes $\mathbf{3^R}$ (R = Me, iPr) underwent clean conversion to give {*fac*-Re(CO)$_3$[Me($\mathbf{L^R}$)]}(I), $\mathbf{4^R}$, over the course of about four hours, detected by both NMR and IR (Table 2) spectroscopy.

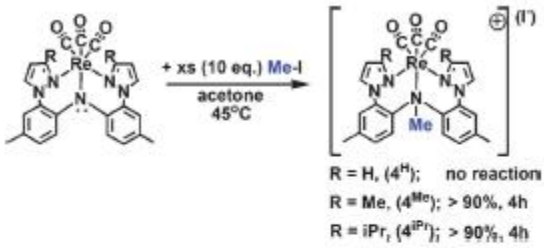

Scheme 2 Attempted reactions of $\mathbf{3^R}$ with MeI intended to form {*fac*-Re(CO)$_3$[Me($\mathbf{L^R}$)]}(I), $\mathbf{4^R}$ complexes.

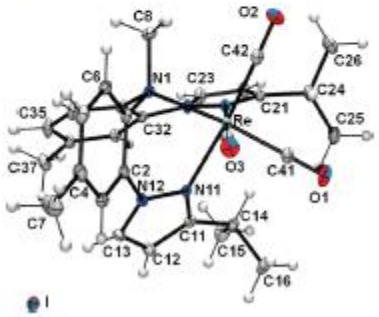

Fig. 9 Structure of {*fac*-Re(CO)$_3$[Me($\mathbf{L^{iPr}}$)]}(I)·2CH_2Cl_2, $\mathbf{4^{iPr}}$·2CH_2Cl_2 with solvate molecules removed for clarity.

Complex 3H failed to react with MeI even after days under similar reaction conditions (of temperature and reagent concentrations). The NMR spectrum of each $\mathbf{4^R}$ shows two sets of resonances for pyrazolyl and tolyl hydrogens whereas that of $\mathbf{3^R}$ shows only one set. Additionally, the solution IR spectrum (CH_2Cl_2) of $\mathbf{4^R}$ exhibited C–O stetching bands with avg. ν_{CO} ~ 1960 cm^{-1} which is comparable to that of $\mathbf{2^R}$. Single crystal X-ray diffraction of $\mathbf{4^{iPr}}$ (Fig. 9) confirmed that the methyl group was indeed bound to the central

Dalton Transactions, Vol. 40, No. 35 (September 2011): pg. 8776-8787. DOI.

nitrogen of the ligand rather than to a pyrazolyl nitrogen. Also, in contrast to the 1^{iPr} where the bromide was bound to rhenium, the iodide in 4iPr is a spectator ion and the ligand binds rhenium in a κ^3N-manner similar to that in $\mathbf{2^{iPr}}$. The greater steric profile of an methyl versus a hydrogen bound to nitrogen subtly impacts the cation structure by increasing the bond distances around rhenium and distorting the ligand framework (by comparing values in Table 1).[13]

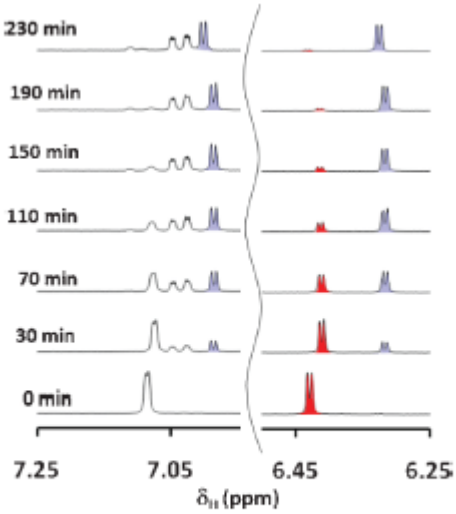

Fig. 10 Portions of the ^{1}H NMR spectra obtained by heating a 1 : 10 mixture of $\mathbf{3^{Me}}$: MeI, highlighting resonances for 4-pyrazolyl hydrogens of $\mathbf{3^{Me}}$ (red-shaded doublet near $\delta_H = 6.4$ ppm) and of the product $\mathbf{4^{Me}}$ (two indigo-shaded doublets near $\delta_H = 7.0$ and 6.3 ppm).

The resonances for various 3-organopyrazolyl hydrogens for $\mathbf{3^R}$ (R = Me, iPr) and the corresponding $\mathbf{4^R}$ products are sufficiently well separated to allow for a convenient means to monitor the rates of reaction by using relative integration of signals (Fig. 10).

Dalton Transactions, Vol. 40, No. 35 (September 2011): pg. 8776-8787. DOI.

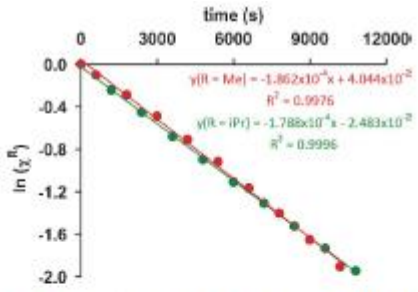

Fig. 11 Pseudo-first order plots of ln (mol fraction of $\mathbf{3^R}$) (R = Me, red; R = iPr, green) *versus* time from integration of 4-pyrazolyl hydrogen NMR resonances observed during conversions of $\mathbf{3^R}$ to $\mathbf{4^R}$ with MeI.

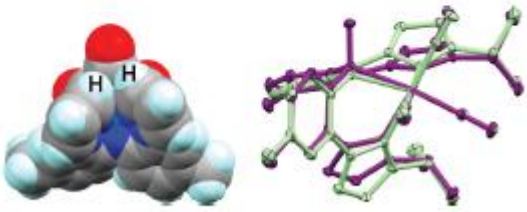

Fig. 12 Left: Space-filling diagram of $\mathbf{3^H}$; Right: Overlay of structures for $\mathbf{3^{iPr}}$ (light green) and the cation in $\mathbf{4^{iPr}}$ (violet) referenced to common ReC_3 cores.

As illustrated in Fig. 11, the pseudo-first order conditions ([MeI]/[$\mathbf{3^R}$] ≥ 10) gave straight-line plots with statistically identical half-lives; t1/2 of 62 (± 3) min for $\mathbf{3^{Me}}$ and 65 (± 3) min for $\mathbf{3^{iPr}}$ where the uncertainty arises from the measurements of different types of resonances within the same experiment. In accord with eqn (1) and the experimental conditions, the corresponding second-order rate

$$-d[\mathbf{3^R}]/dt = k_{obs}[\mathbf{3^R}] = {}_{k2}[MeI][\mathbf{3^R}] \qquad (1)$$

constants were found to be k_2 = 5.7 ¥ 10^{-4} $M^{-1}s^{-1}$ for 0.033 M $\mathbf{3^{Me}}$ and 0.331 M MeI and k_2 = 8.4 ¥ 10^{-4} $M^{-1}s^{-1}$ for 0.021 M $\mathbf{3^{iPr}}$ and 0.212 M MeI. More in-depth kinetic analysis of these and other related systems is underway.

The difference in reactivity between the various 3-organopyrazolyl derivatives $\mathbf{3^R}$ and that of $\mathbf{3^H}$ can be attributed to inter-related structural and electronic factors. It was anticipated and found that the replacement of the two (very close) hydrogen atoms labeled in Fig. 12 with any other group should (and does) drastically alter the structure and reactivity of the complexes. Given the typical inert nature of Re-ligand bonds, the spectroscopic data, and that no N-

Dalton Transactions, Vol. 40, No. 35 (September 2011): pg. 8776-8787. DOI.

methyl pyrazolyls was detected in reactions with MeI, it is expected that the ligands remain tridentate in acetone solutions of $\mathbf{3^H}$ and $\mathbf{3^R}$ and that pyrazolyl dissociation is unlikely the origin of increased reactivity of $\mathbf{3^R}$ versus $\mathbf{3^H}$. If the ligands are indeed tridentate, the greater reactivity of $\mathbf{3^R}$ versus $\mathbf{3^H}$ toward MeI can be rationalized by the greater steric accessibility of the more pyramidal nitrogen of $\mathbf{3^R}$ to incoming electrophiles than that in $\mathbf{3^H}$. The pyramidal nature of nitrogen in $\mathbf{3^R}$ has two consequences. First, the complexes $\mathbf{3^R}$ are pre-organized in a conformation similar to that found for $\mathbf{4^R}$ (right of Fig. 12); the activation barrier for the conversion of $\mathbf{3^H}$ to hypothetical $\mathbf{4^H}$ should be higher due to requisite structural reorganization. Moreover, the basicity of the amido nitrogen in $\mathbf{3^R}$ is also expected to be greater owing to the greater s-character, lower degree of conjugation and the slightly higher energy HOMO versus $\mathbf{3^H}$ (Fig. 8).

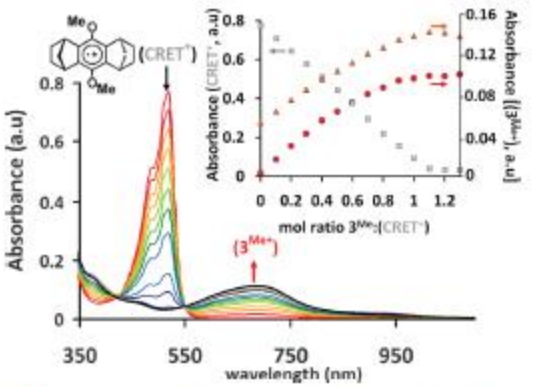

Fig. 13 Spectroelectrochemical titration reaction between 3^{Me} and $(CRET^+)(SbCl_6^-)$ in CH_2Cl_2. Inset: Plot of absorbance *versus* mol ratio monitoring bands for $(CRET^+)$ at 518 nm (grey squares) and for (3^{Me+}) at 377 nm (orange triangles) and 687 nm (red circles).

The discrepancy in properties and reactivity between $\mathbf{3^R}$ (R = Me, iPr) and $\mathbf{3^H}$ perpetuates in the one-electron oxidized products $(3^{R+})(SbCl_6\text{-})$. Reactions of $\mathbf{3^R}$ with the organic cation radical 9,10-dimethoxyocta-hydro-1,4:5,8-dimethanoanthracenium hexachloroantimonate $[(CRET^+)(SbCl_6\text{-})]$,14 a modest oxidant (E1/2,red 0.58 V vs. Fc/Fc+), affords blue-green $(3^{R+})(SbCl_6\text{-})$, see Fig. 13 and ESI. While $(\mathbf{3^{H+}})$ was found to be stable as a solid and only very slowly decomposed at 295 K in aerated CH_2Cl_2 ($t_{1/2}$ = 3d), $(\mathbf{3^{R(= Me\ or\ iPr}}+)(SbCl_6\text{-})$ decomposed much more rapidly in aerated CH_2Cl_2 ($t_{1/2}$ = 3.5 h for both); thus, solution measurements must

Dalton Transactions, Vol. 40, No. 35 (September 2011): pg. 8776-8787. DOI.

be made on freshly prepared samples with exclusion of air. At 295 K, the EPR spectrum of each cation radical (**3**$^{R+}$) in CH_2Cl_2 (Fig. 14) displays a well-resolved sextet signal due to the hyperfine interaction between the electronic spin and the $^{185/187}$Re nuclei (I = 5/2). The isotropic signal for (**3**$^{H+}$) (g_{iso} = 2.017 a_{Re} 49.5G) is similar but distinct from the signals for either (**3**$^{Me+}$) (g_{av} = 2.016, a_{Re} = 33.4 G, a_N = 7.5 G) or (**3**$^{iPr+}$) (g_{av} = 2.016, a_{Re} = 33.8 G, a_N = 7.5 G).

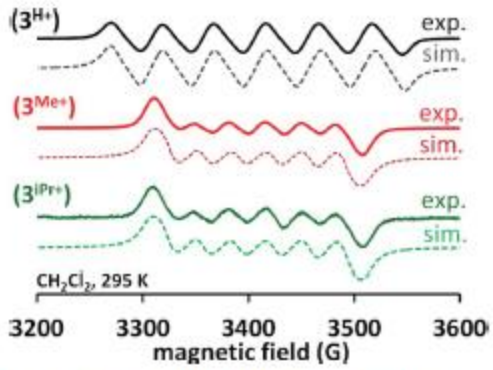

Fig. 14 Comparison of X-Band (9.63 GHz, 295 K) EPR spectra for (3^{R+})($SbCl_6^-$) in CH_2Cl_2 (R = H, black; R = Me, red; R = iPr, green). Simulated spectra have dashed lines.

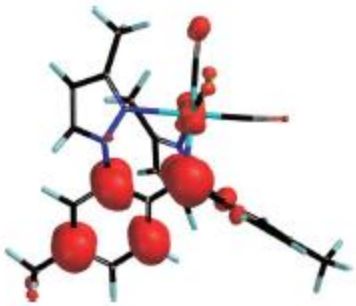

Fig. 15 Spin density isosurface for energy minimized (BP86) structural model of (3^{Me+}) from theoretical calculations (UB3LYP/LACVP).

In each case, the relatively small deviation of g-values from that for the free electron g_e = 2.0023 and the small hyperfine couplings are consistent with a ligand-centred rather than a metal-centred radical, with the spin density on rhenium being highest for (**3**$^{H+}$).[3,15] Theoretical calculations indicate most of the spin density is located on the ligand (Fig. 15) in accord with other experimental indicators of a ligand-centred radical such as the occurrence of intense piradical bands (π(L) → SOMO) in the 650–750 nm range of the electronic

absorption spectrum. Also, the average energy of the C–O stretching bands in the solution (CH_2Cl_2) IR spectra, ν_{co}(avg), increases by only 33, 37, and 41 cm^{-1} on traversing between $\mathbf{3^R}$ and $\mathbf{3^{R+}}$ for R = H, Me, and iPr, respectively (Table 2). Such a relatively small increase in energy is similar to the 38 cm^{-1} increase for related PNP pincer complexes $[Re(CO)_3(PNP)]^{n+}$ (n = 0,1) (measured for KBr pellets) and is consistent with ligand-centered oxidation.[2] Rhenium-centred oxidations would be expected to have ν_{co}(avg) increase on the order of 50–100 cm^{-1}.[2,3,1] A final set of poorly understood observations that highlight the incongruent reactivity patterns of $\mathbf{3^R}$ (R = Me, iPr) and $\mathbf{3^H}$ derivatives is thatCH_2Cl_2 solutions of $\mathbf{3^{Me}}$ or $\mathbf{3^{iPr}}$ were light sensitive but those of $\mathbf{3^H}$ were not. Thus, CH_2Cl_2 solutions of the latter two compounds should be protected from light and measurements should be made on freshly prepared solutions. A more extended account of the unexpected photodecomposition behaviour can be found in the Electronic Supporting Information.

Conclusions

The purpose of this study was to investigate whether the reactivity of tricarbonylrhenium(I) complexes of di(2-(3-R-pyrazolyl)-ptolyl) amine derivatives would be altered by substitution at the 3-pyrazolyl position; the properties of various $Re(CO)_3$ complexes of the unsubstituted ligand H($\mathbf{L^R}$) R = H were communicated previously. To this end, two new 3-alkylpyrazolyl ligands (R = Me, iPr) were prepared in good yield by straightforward CuIcatalyzed amination reactions. The availability of the three H($\mathbf{L^R}$) ligands (R = H, Me, and iPr) ligands allowed a series of nine tricarbonylrhenium(I) complexes to be prepared and fully characterized both in solution and the solid state. The most significant structural and reactivity differences were found across the series of *fac*-$Re(CO)_3$($\mathbf{L^R}$) ($\mathbf{3^R}$) complexes with deprotonated, formally uninegative, NNN-ligands. The bond distances in $\mathbf{3^R}$ increased with increasing steric bulk of the 3-pyrazolyl substituents.For $\mathbf{3^H}$, a conformation with near C_s symmetry and a planar amido nitrogen was found in the solid state whereas for $\mathbf{3^{Me}}$ or $\mathbf{3^{iPr}}$, the ligands were greatly distorted with substantial pyramidalization of the amido nitrogen. This conformation is dictated by unfavorable steric interactions that would occur between 3-pyrazolyl substituents in a pseudo-Cs symmetric conformation such as

Dalton Transactions, Vol. 40, No. 35 (September 2011): pg. 8776-8787. DOI.

in $\mathbf{3^H}$. The solution spectroscopic data demonstrate that none of the three complexes retain their static solid state geometries. Based on comparisons with other complexes, this behavior is attributed to conformational changes of intact complexes with tridentate ligands. Pyrazolyl dissociation to give bidentate ligands and perhaps a coordinatively unsaturated (or weakly-solvated)metal centers cannot be excluded in either $\mathbf{2^R}$ or $\mathbf{3^R}$ cases (which show dynamic solution behavior), but seems unlikely owing the usual kinetically inert nature of rhenium-ligand bonds, the flexibility of six-membered chelate rings, combined with the observed reactivity patterns. The relative reactivities follow the divisive pattern where $\mathbf{3^{Me}}$ and $\mathbf{3^{iPr}}$ are reactive towards MeI to afford an N-methyl (amino not pyrazolyl) derivative but $\mathbf{3^H}$ does not react with MeI under similar conditions. Moreover, CH_2Cl_2 solutions of the former two complexes are photosensitive but similar solutions of $\mathbf{3^H}$ were photo-stable. A final difference was found for the one-electron oxidized products ($\mathbf{3^{R+}}$); the room-temperature EPR spectrum of CH_2Cl_2 solutions for R = Me or iPr gave signals indicative of a more asymmetric ligand environment than that for R = H. Moreover, solutions of ($\mathbf{3^{Me+}}$) and ($\mathbf{3^{iPr+}}$) were considerably more prone to decomposition than ($\mathbf{3^{H+}}$). The incongruent nature of the structures and electronic spectra of the two classes of complexes combined with results of DFT calculations for the various $\mathbf{3^R}$ and ($\mathbf{3^{R+}}$) cation radicals indicate that the differences arise from a combination of the lower degree of conjugation across the ligand backbone and a (surprising) greater accessibility to a more pyramidal amido nitrogen on the ligand. Studies are underway to further explore the chemical and photochemical potential of these and related complexes.

Experimental

Materials

Pyrazole, 3-methylpyrazole, CuI, N,N'-dimethylethylenediamine (DMED), anhydrous K_2CO_3 powder, and (NE_{t4})(OH) (1 M in MeOH) were purchased from commercial sources and used without further purification while $Re(CO)_5Br$,[17] di(2-bromo-*p*-tolyl) amine,[5] 3 isopropylpyrazole[6] were prepared by literature methods. Methyl iodide was distilled under vacuum before use. Solvents used in the

Dalton Transactions, Vol. 40, No. 35 (September 2011): pg. 8776-8787. DOI.

preparations were dried by conventional methods and were distilled under nitrogen prior to use.

Instrumentation

MidwestMicroLab, LLC, Indianapolis, Indiana 45250, performed all elemental analyses. ^{1}H and ^{13}C NMR spectra were recorded on a Varian 400 MHz spectrometer. Chemical shifts were referenced to solvent resonances at δ_H 7.27, δC 77.23 for $CDCl_3$; δH 5.32, δC 54.00 for CD_2Cl_2 and δH 2.05, δC 29.92 for acetone-d_6. Melting point determinations were made on samples contained in glass capillaries using an Electrothermal 9100 apparatus and are uncorrected. Infrared spectra were recorded on samples a KBr pellets and as CH_2Cl_2 solutions using a Nicolet Magna-IR 560 spectrometer. Absorption measurements were recorded on an Agilent 8453 spectrometer. Electrochemical measurements were collected under nitrogen atmosphere at a scan rate of 100 mV s^{-1} for samples as 0.1 mM CH_2Cl_2 solutions with 0.1 M NBu_4PF_6 as the supporting electrolyte. A three-electrode cell comprised of an Ag/AgCl electrode, a platinum working electrode, and a glassy carbon counter electrode was used for the voltammetric measurements. With this set up, the ferrocene/ferrocenium couple had an $E_{1/2}$ value of +0.53 V consistent with the literature value in this solvent.18 Mass spectrometric measurements recorded in ESI(+) or ESI(-) mode were obtained on a Micromass Q-TOF spectrometer whereas those performed by using direct-probe analyses were made on a VG 70S instrument. For the ESI(+) experiments formic acid (approximately 0.1% v/v) was added to the mobile phase (CH^3CN). EPR measurements were obtained using a Bruker ELEXSYS E600 equipped with an ER4116DM cavity resonating at 9.63 GHz, an Oxford Instruments ITC503 temperature controller and ESR-900 helium-flow cryostat. The ESR spectra were recorded with 100 kHz field modulation.

*Di(2-(3-methylpyrazolyl)-p-tolyl)amine, H(**L^{Me}**)*

A reaction vessel was charged with a mixture of 3.44 g (9.69 mmol) di(2-bromo-*p*-tolyl)amine, 2.78 g (33.9 mmol, 3.5 equiv) 3-methylpyrazole, 5.35 g (38.7 mmol, 4.0 equiv)K2CO3, and 0.38mL (3.87 mmol, 40 mol %) DMED, and was deoxygenated by three

Dalton Transactions, Vol. 40, No. 35 (September 2011): pg. 8776-8787. DOI.

evacuation and nitrogen back-fill cycles. Then, 0.18 g (0.97 mmol, 10 mol %) CuI was added as a solid under nitrogen. The reaction mixture was heated under nitrogen at 200°C for 15 h. After cooling to room temperature, 200 mL of H_2O was added and the mixture was extracted with three 100 mL portions of CH_2Cl_2. The combined organic layers were dried over$MgSO_4$, filtered, and solvent was removed by rotary evaporation to give an oily residue that was purified by column chromatography on silica gel. Elution with 8 : 1 hexanes:ethyl acetate (R_f 0.7) afforded 2.28 g (66%) of H(**L^{Me}**) as a white solid. Mp, 83–85°C. Anal. Calcd (obs.) for $C_{22}H_{23}N_5$: C, 73.92 (73.68); H, 6.49 (6.53); N, 19.59 (19.41). IR (KBr) ν_{NH} 3297. ^{1}H NMR: (CD_2Cl_2) 8.43 (s, 1H, NH), 7.62 (d, *J* = 2 Hz, 2H, H_5pz), 7.22 (d, *J* = 8 Hz, 2H, Ar), 7.09 (s, 2H, Ar), 7.00 (d, *J* = 8 Hz, 2H, Ar), 6.19 (d, *J* = 2 Hz, 2H, H_4pz), 2.29 (s, 12H, CH3). $_1$HNMR: (acetone-d_6) 8.86 (s, 1H, NH), 7.85 (d, *J* = 2 Hz, 2H, H_5pz), 7.24 (d, *J* = 8 Hz, 2H, Ar), 7.19 (s, 2H, Ar), 7.05 (d, *J* = 8 Hz, 2H, Ar), 6.24 (d, *J* = 2, 2H, H_4pz), 2.29 (s, 6H, ArCH_3), 2.28 (s, 6H, pzCH_3). ^{13}C NMR: ($CDCl_3$) 149.9, 134.6, 131.0, 130.7, 130.2, 128.8, 125.8, 118.9, 106.6, 20.7, 13.8. UV-VIS λ_{max}, nm (ε, $M^{-1}cm^{-1}$), CD_2Cl_2: 242(37149), 304(26376). Single crystals suitable for X-ray diffraction were obtained by slow evaporation of a hexane solution.

*Di(2-(3-isopropylpyrazolyl)-p-tolyl)amine, H(**L^{iPr}**)*

In a manner similar to that described above, a mixture of 7.17 g (0.0202 mol) di(2-bromo-p-tolyl)amine, 7.78 g (0.0706 mol, 3.5 equiv) 3-isopropylpyrazole, 11.05 g (0.0800 mol, 4.0 equiv)K_2CO_3, and 0.79 mL (0.65 g, 7.4 mmol, 35 mol %) DMED, 0.38 g (2.0 mmol, 10 mol %) CuI afforded 5.06 g (61%) ofH(**L^{iPr}**) as a light yellow oil after workup and purification (SiO2, 8 : 1 Hexane: ethyl acetate R_f 0.6). Anal. Calcd (obs.) for $C_{26}H_{31}N_5$: C, 75.51 (75.61);s H, 7.56 (7.48); N, 16.93 (16.78). IR (KBr) ν_{NH} 3296. ^{1}H NMR: (CD_2Cl_2) 8.82 (s, 1H, NH), 7.67 (d, J = 2 Hz, 2H, H_5pz), 7.18 (d, J = 2 Hz, 2H, Ar), 7.14 (s, 2H, Ar), 6.98 (dd, J = 8, 2 Hz, 2H, Ar), 6.21 (d, J = 2 Hz, 2H, H_4pz), 2.95 (sept, J = 7 Hz, 2H, Me_2 CH), 2.29 (s, 6H, ArCH_3), 1.22 (d, J = 1 Hz, 6H, iPrCH_3), 1.20 (d, *J* = 1 Hz, 6H, iPrCH_3). 1H NMR: (acetone-d6) 8.70 (s, 1H, NH), 7.87 (d, *J* =2Hz, 2H, H5pz), 7.23 (s, 2H, Ar), 7.20 (d, *J* =8Hz, 2H, Ar), 7.01 (d, *J* =8Hz, 2H, Ar), 6.28 (d, *J* =2Hz, 2H, H_4pz), 2.99 (sept,

Dalton Transactions, Vol. 40, No. 35 (September 2011): pg. 8776-8787. DOI.

J = 7 Hz, 2H, Me_2CH), 2.29 (s, 6H, $ArCH_3$), 1.24 (d, *J* = 1 Hz, 6H, $iPrCH_3$), 1.22 (d, *J* = 1 Hz, 6H, $iPrCH_3$), ^{13}C NMR: ($CDCl_3$) 160.4, 134.3, 130.9, 130.5, 129.9, 128.5, 125.6, 119.3, 103.7, 27.9, 22.9, 20.7. UV-VIS λ_{max}, nm (ϵ, $M^{-1}cm^{-1}$), CD^2Cl_2: 244(36386), 304(22429).

$ReBr(CO)_3[\mathbf{H}(L^{Me})]$, ($\mathbf{1^{Me}}$)

A mixture of 0.172 g (0.423 mmol) $Re(CO)_5Br$ and 0.151 g (0.422 mmol) of **H**(**L^{Me}**) in 20 mL of toluene was heated at reflux 15h. The resulting precipitate was isolated by filtration, washed with two 5 mL portions Et_2O and dried under vacuum which afforded 0.22 g (75%) **1^{Me}** as a fine white powder. Mp, 269–271°C dec. Anal. Calcd (obs.) for $C_{25}H_{23}BrN_5O_3Re$: C, 42.44 (42.20); H, 3.28 (3.21); N, 9.90 (9.74). IR (KBr) ν_{NH} 3138; ν_{co} 2025, 1915, 1895 cm^{-1}. 1H NMR: (CD_2Cl_2, 303 K) three species, see text: **I**, 88% of signal integration intensity from resolved resonances in the R–CH_3, NH, H_5pz and H4pz regions of spectrum; **II**, 10% of signal; **III** 2% of signal): 12.10 (br s, 1H, NH, III), 11.84 (br s, 1H, NH, **II**), 10.50 (br s, 1H, NH, **I**), 8.06 (d, *J* = 2 Hz, 1H, H_5pz, **I**), 8.03 (d, *J* = 2 Hz, 1H, H_5pz, **II**), 7.89 (d, *J* = 2 Hz, 1H, H_5pz, **II**), 7.79 (d, *J* = 2 Hz, 1H, H_5pz, **I**), 7.58 (d, *J* = 8 Hz, 1H, Ar, **I**), 7.33–7.24 (m, 4H, Ar, **I**/**II**/**III**), 7.21–7.02 (br m, 4H, Ar I/II/III), 6.60 (d, *J* = 2 Hz, 1H, H_4pz, **II**), 6.59 (d, *J* = 2 Hz, 1H, H_4pz, **I**), 6.31 (d, J = 2 Hz, 1H, H4pz, **II**), 6.20 (d, *J* = 2 Hz, 1H, H_4pz, **I**), 2.74 (s, 3H, $pzCH_3$, **I**), 2.47 (s, 3H, $ArCH_3$, **I**), 2.44 (s, 3H, $ArCH_3$, **I**), 2.41–2.28 (br m, 9H, pz- and $ArCH_3$, II/III), 2.21 (s, 3H, $pzCH_3$, **II**), 1.98 (s, 3H, $pzCH_3$, **I**). ^{1}H NMR: (CD_2Cl_2, 213 K) 11.70 (br s, 1H, NH, **III**), 11.48 (br s, 1H, NH, **II**), 10.29 (br s, 1H, NH, **I**), 8.17 (d, *J* = 8 Hz, 1H, Ar, **II**), 8.13 (br s, 1H, H_5pz, **III**), 8.08 (br s, 1H, H_5pz, **I**), 7.99 (br s, 1H, H_5pz, **II**), 7.95 (br s, 1H, H_5pz, **III**), 7.86 (br s, 1H, H5pz, II), 7.80 (d, J = 8 Hz, 1H, Ar, I), 7.74 (br s, 1H, H_5pz, **I**), 7.53 (br s, 1H, Ar, **II**), 7.41–7.01(br m, see text, Ar, **I**/**II**/**III**), 6.91 (s, 1H, Ar, **II**), 6.83 (d, *J* =8Hz, 1H, Ar, **II**), 6.61 (d, *J* = 2 Hz, 1H, H_4pz, **II**), 6.58 (d, *J* = 2 Hz, 1H, H_4pz, **I**), 6.38 (br s, 1H, H_4pz, **III**), 6.31 (d, *J* = 2 Hz, 1H, $H4_{pz}$, **II**), 6.18 (br s, 1H, H_4pz, **III**), 6.16 (br s, 1H,H4pz, **I**), 6.07 (d, *J* =2Hz, 1H, H_4pz, **II**), 5.87 (1H, H_4pz, **III**), 2. 78 (s, 3H, $pzCH_3$, **II**), 2.73 (s, 3H, $pzCH_3$, **III**), 2.68 (s, 3H, $pzCH_3$, I), 2.62 (s, 3H, $pzCH_3$, III), 2.45 (s, 3H,

Dalton Transactions, Vol. 40, No. 35 (September 2011): pg. 8776-8787. DOI.

$ArCH_3$, **II**), 2.44 (s, 3H, $ArCH_3$, I), 2.39 (s, 3H, $ArCH_3$, I), 2.33 (s, 3H, $ArCH_3$, **III**), 2.24 (s, 3H, $ArCH_3$, **III**), 2.18 (s, 3H, $ArCH_3$, **II**), 2.02 (s, 3H, $pzCH_3$, **II**), 1.83 (s, 3H, $pzCH_3$, **I**). UV-VIS λ_{max}, nm (ε, $M^{-1}cm^{-1}$), CD_2Cl_2: 231(50963), 261(34522), 289(11818). X-ray quality crystals of $\mathbf{1^{Me}}$·acetone were grown by layering an acetone solution with hexane and allowing the solvents to slowly diffuse over two days.

$ReBr(CO)_3[\mathbf{H}(\mathbf{L^{iPr}})]$ ($\mathbf{1^{iPr}}$)

A mixture of 0.256 g (0.630 mmol) $Re(CO)_5Br$ and 0.260 g (0.727 mmol) of **H**($\mathbf{L^{iPr}}$) in 20mL of toluene was heated at reflux for 15 h. The resulting precipitate was isolated by filtration, washed with two 5 mL portions Et_2O and dried under vacuum which afforded 0.34 g (71%) as a fine white powder. Mp, 264–267°C dec. Anal. Calcd (obs.) $C_{29}H_{31}BrN_5O_3Re$: C, 45.61 (45.40);H, 4.09 (3.96);N, 9.17 (9.14). IR (KBr) ν_{NH} 3143; ν_{co} 2020, 1910, 1880 cm^{-1}. ^1H NMR: (CD_2 Cl_2, 293 K) two species, see text: **I**, 92% of signal integration intensity from resolved resonances in the R–CH3, NH, H_5pz and H_4pz regions of spectrum; **II**, 8% of signal: 11.96 (br s, 1H, NH, **II**), 10.50 (br s, 1H, NH, **I**), 8.08 (d, *J* = 2.9Hz, 1H,H_5pz, **I**), 8.06 (brm, 1H,H_5pz, **II**), 7.90 (d, *J* = 2.5Hz, 1H,H_5pz, II), 7.82 (d, *J* = 2.5 Hz, 1H, H_5pz, I), 7.63 7.53 (br s, 6H, Ar, **II**), 7.29 (m, 3H, Ar, **I**), 7.18 (m, 3H, Ar, **I**), 6.65 (d, *J* = 2.9 Hz, 1H, H_4pz, **II**), 6.64 (d, *J* = 2.9 Hz, 1H, H_4pz, **I**), 6.37 (br m, 1H, H_4pz, **II**), 6.25 (d, *J* = 2.5 Hz, 1H, H_4pz, **I**), 3.85 (sept, *J* = 7.1 Hz, 1H, Me_2CH, **I**), 2.51 (sept, J = 6.7 Hz, 1H, Me2CH, II), 2.46 (s, 3H, ArCH3, **I**), 2.43 (s, 3H, $ArCH_3$, **I**), 2.38 (br s, 3H, $ArCH_3$, **II**), 1.33 (d, *J* = 7 Hz, 3H, $iPrCH_3$, *I*), 1.29 (d, *J* = 7 Hz, 3H, $iPrCH_3$, **I**), 1.23 (brm, 3H, $iPrCH_3$, **II**), 1.04 (d, *J* = 7 Hz, 3H, $iPrCH_3$, **I**), 0.99 (d, *J* = 7 Hz, 3H, $iPrCH_3$, **I**), 0.88 (br m, 3H, $iPrCH_3$, **II**). UV-VIS λ_{max}, nm (ε,$M^{-1}cm^{-1}$), CD_2Cl_2: 295 (10,900), 259 (38,200), 230 (51,500). ^{13}CNMR: (CD_2Cl_2) 168.3, 161.7, 138.6, 137.5, 133.5, 130.6, 130.5, 129.4, 127.3, 125.2, 121.8, 107.2, 105.1, 31.1, 28.4, 24.3, 23.4, 23.1, 22.8, 21.3, 20.9. X-ray quality crystals were grown by layering an acetone solution with hexane and allowing the solvents to slowly diffuse over two days.

Dalton Transactions, Vol. 40, No. 35 (September 2011): pg. 8776-8787. DOI.

*{Re(CO)$_3$[**H**(**L^{Me}**)]}(PF6), (**2^{Me}**)*

A mixture of 0.075 g (0.11 mmol) of **1^{Me}** and 0.04 g (0.11 mmol) of $TlPF_6$ in 10 mL dry CH_3CN was heated at reflux overnight. After cooling to room temperature TlBr was separated by filtration through Celite, and solvent was removed by rotary evaporation. The residue was washed with two 5 mL portions Et_2O and was dried under vacuum to give 0.060 g (75%) of **2^{Me}** as a colorless to pale yellow powder.

Mp, 243–246°C dec. Anal. Calcd (obs.) for $C_{26}H_{25}Cl_2F_6N_5O_3PRe$ (**2^{Me}**·CD_2Cl_2): C, 36.41 (36.25); H, 2.94 (2.77); N, 8.17 (8.27). IR (KBr) ν_{NH} 3253; ν_{co} 2030, 1940, 1920 cm^{-1}. ^1H NMR: (CD_2Cl_2, 233 K) 7.98 (d, *J* = 3 Hz, 1H, H_5pz), 7.54 (s, 1H, NH), 7.53 (d, *J* = 3 Hz, 1H, H_5pz), 7.48 (d, *J* = 8 Hz, 1H, Ar), 7.41 (d, *J* = 8 Hz, 1H, Ar), 7.30 (s, 1H, Ar), 6.94 (s, 1H, Ar), 6.89 (d, *J* = 9 Hz, 1H, Ar), 6.69 (d, *J* = 9 Hz, 1H, Ar), 6.66 (d, *J* = 3 Hz, 1H, H_4pz), 6.10 (d, *J* = 3 Hz, 1H, H_4pz), 2.80 (s, 3H, $pzCH_3$), 2.49 (s, 3H, $ArCH_3$), 2.23 (s, 3H, $ArCH_3$, $ArCH_3$), 2.04 (s, 3H, $pzCH_3$). ^{13}C NMR: (CD_2Cl_2, 295 K) no signals were observed even after prolonged acquisition times. UV-VIS λ_{max}, nm (ε, $M^{-1}cm^{-1}$), CD_2Cl_2: 230(34154), 250 (28087), 294 (8854). X-ray quality crystals were grown by layering an acetone solution with hexane and allowing the solvents to slowly diffuse over two days.

*{Re(CO)$_3$[**H**(**L^{iPr}**)]}(PF$_6$), (**2^{iPr}**)*

A mixture of 0.205 g (0.27 mmol) of **1^{iPr}** and 0.084 g (0.27 mmol) $TlPF_6$ in 20 mL dry THF was heated at reflux overnight. After cooling to room temperature, TlBr was separated by filtration through Celite and solvent was removed from the filtrate by rotary evaporation. The residue was washed with two 5 mL portions Et_2O and was dried under vacuum to give 0.198 g (84%) of **2^{iPr}** as a white powder. Mp, 278–280°C dec. Anal. Calcd (obs.) for $C_{29}H_{31}F_6N_5O_3PRe$: C, 42.03 (42.26); H, 3.77 (4.02); N, 8.45 (8.12) IR (KBr) ν_{NH} 3236; ν_{co} 2035, 1940, 1911 cm^{-1}. ^1H NMR: (CD_2Cl_2, 233 K) 8.24 (s, 1H, NH), 7.97 (d, *J* = 3 Hz, 1H, H_5pz), 7.56 (d,

Dalton Transactions, Vol. 40, No. 35 (September 2011): pg. 8776-8787. DOI.

J = 3 Hz, 1H, H_5pz), 7.55 (d, *J* = 8 Hz, 1H, Ar), 7.40 (d, *J* = 8 Hz, 1H, Ar), 7.29 (s, 1H, Ar), 6.90 (s, 1H, Ar), 6.87 (d, *J* = 8.5 Hz, 1H, Ar), 6.73 (d, *J* = 3 Hz, 1H, H_4pz), 6.70 (d, *J* = 8.5 Hz, 1H, Ar), 6.15 (d, J = 3 Hz, 1H, H_4pz), 3.84 (sept, J = 7 Hz, 1H, Me_2CH), 2.92 (sept, J = 7 Hz, 1H, Me_2CH), 2.49 (s, 3H, $ArCH_3$), 2.23 (s, 3H, $ArCH_3$), 1.49 (d, *J* = 7 Hz, 3H, $iPrCH_3$), 1.36 (d, *J* = 7 Hz, 3H, $iPrCH_3$), 1.16 (d, *J* = 7 Hz, 3H, $iPrCH_3$), 0.62 (d, *J* = 7 Hz, 3H, iPrCH3). 13C NMR: (CD2Cl2, 295 K) no signals were observed even after prolonged acquisition times. UV-VIS λ_{max}, nm (ε, $M^{-1}cm^{-1}$), CD_2Cl_2: 229(31536), 249(24891), 294(5514). X-ray quality crystals were grown by layering an acetone solution with hexane and allowing the solvents to slowly diffuse over two days.

*Re(CO)$_3$(**L^{Me}**), (**3^{Me}**)*

Method A. To a solution of 0.201 g (0.28 mmol) **1^{Me}** in 20 mL of CH_3CN was added 2.75 mL (0.283 mmol) (NEt4)(OH) solution in MeOH immediately giving a yellow solution. The mixture was stirred for 30 min then solvent was removed by rotary evaporation. The yellow residue was washed with two 5 mL portions MeOH and was dried under vacuum to leave 0.150 g (88%) of **3^{Me}** as a yellow powder. Mp, 250–254°C dec. Anal. Calcd (obs.) for $C_{25}H_{22}N_5O_3Re$: C, 47.91 (48.01); H, 3.54 (3.58); N, 11.18 (11.23). IR (KBr) ν_{co} 2020, 1905, 1885 cm^{-1}. ^{1}H NMR: (CD_2Cl_2, 293 K) 7.81 (d, *J* = 2 Hz, 2H, H_5pz), 6.92 (s, 2H, Ar–H), 6.90 (part of AB d, 2H, Ar), 6.63 (part of AB d, 2H, Ar), 6.28 (d, *J* = 2 Hz, 2H, H_4pz), 2.52 (s, 6H, $pzCH_3$), 2.27 (s, 6H, $ArCH_3$). ^{1}H NMR: (acetone-d6) 8.26 (d, *J* = 3 Hz, 2H, H_5pz), 7.10 (d, *J* = 2 Hz, 2H, Ar), 6.92 (part of AB d, J = 8, 2 Hz, 2H, Ar), 6.61 (part of AB d, *J* = 8 Hz, 2H, Ar), 6.44 (d, J = 3 Hz, 2H, H_4pz), 2.53 (s, 6H, $pzCH_3$), 2.23 (s, 6H, $ArCH_3$). ^{13}C NMR: (CD_2Cl_2) 198.2, 196.7, 155.5, 149.8, 132.2, 131.5, 129.6, 128.2, 124.2, 122.1, 108.3, 20.6, 17.1. UV-VIS λ_{max}, nm (ε, $M^{-1}cm^{-1}$), CD^2Cl^2: 234(44756), 247(41711), 298(14615), 392(3687). X-ray quality crystals were grown by layering an acetone solution with hexane and allowing the solvents to slowly diffuse over two days.

Method B. A 0.32 mL aliquot of 0.509 M (NEt_4)(OH) (0.16 mmol) in MeOH was added to a solution of 0.124 g (0.160 mmol) **2^{Me}** in 10 mL of CH_3CN immediately giving a yellow

Dalton Transactions, Vol. 40, No. 35 (September 2011): pg. 8776-8787. DOI.

solution. The mixture was stirred for 15 min then solvent was removed by rotary evaporation. The yellow residue was extracted with three 5 mL portions of benzene and solvent was removed by vacuum distillation to leave a mixture of benzene-soluble **3^{Me}** contaminated with H(**L^{Me}**) (NMR). The contaminant was removed by washing with minimal Et_2O (2 mL), to leave 0.030 g (30%) of **3^{Me}** with characterization data identical to above. Selective precipitation of **3^{Me}** using MeOH as inMethod A, did not lead to improved yield.

*Re(CO)$_3$(**L^{iPr}**), (**3^{iPr}**)*

In a manner similar to method A of 3Me, 0.091 mmol $(NEt_4)(OH)$ (1.3 mL of 0.07 M solution in MeOH) and 0.073 g (0.095 mmol) gave 0.040 g (61%) of 3iPr as a yellow powder. Mp, 240–243° Cdec. Anal. Calcd (obs.) for $C_{29}H_{30}N_5O_3Re$: C, 51.01 (51.24); H, 4.43 (4.54); N, 10.26 (10.22). IR (KBr): ν_{co} 2010, 1900, 1875 cm^{-1}. ^1H NMR (CD_2Cl_2, 293 K) 7.80 (d, *J* = 3 Hz, 2H, H_5pz), 6.89 (s, 2H, Ar), 6.88 (part of AB d, 2H, Ar), 6.60 (part of AB d, 2H, Ar), 6.33 (d, *J* = 3 Hz, 2H, H_4pz), 3.57 (sept, *J* = 7 Hz, 2H, Me_2CH), 2.26 (s, 6H, $ArCH_3$), 1.34 (d, *J* = 7 Hz, 6H, $iPrCH_3$), 1.02 (d, *J* = 7 Hz, 6H, $iPrCH_3$). ^1H NMR: (acetone-d_6) 8.18 (d, *J* =3Hz, 2H, H_5pz), 7.07 (s, 2H, Ar), 6.89 (part of AB d, 2H, Ar), 6.56 (part of AB d, 2H, Ar), 6.55 (d, *J* = 2 Hz, 2H, H_4pz), 3.62 (sept, *J* = 7 Hz, 1H, Me_2CH), 2.22 (s, 6H, $ArCH_3$), 1.37 (d, *J* =7Hz, 6H, $iPrCH_3$), 1.08 (d, *J* =7Hz, 6H, $iPrCH_3$). ^{13}CNMR: (CD_2Cl_2) 197.2, 194.5, 166.0, 150.0, 133.0, 131.5, 129.5, 128.5, 124.4, 122.0, 104.6, 30.6, 23.6, 23.3, 20.6. UV-VIS λ_{max}, nm (ε, $M^{-1}cm^{-1}$), CD_2Cl_2: 234(49162), 247(46362), 305(12127), 391(3667). X-ray quality crystals were grown by layering an acetone solution with hexane and allowing the solvents to slowly diffuse over two days.

General procedure for NMR-scale reactions between 3R and MeI

Solutions were prepared in NMR tubes by dissolving 7–9 mg 3R in 0.35 mL of acetone-d6. A ten-fold excess MeI (7–9 mL, as appropriate) was injected into the solution, the NMR tube was

Dalton Transactions, Vol. 40, No. 35 (September 2011): pg. 8776-8787. DOI.

immediately sealed and inserted into the pre-heated 45°C NMR cavity for measurements where time of insertion served as the reference point (t = 0 min). NMR spectra were acquired at 10 min intervals for the first 30 min, then at 30 min intervals thereafter.

Colorless crystals of {$Re(CO)_3$[Me(**L**^{iPr})]}(I), (**4**^{iPr}) suitable for single-crystal X-ray diffraction were obtained by removing volatile components from the completed reactions by vacuum distillation, dissolving the residue in CH2Cl2, layering with n-hexane, and allowing the solvents to slowly diffuse 15 h.

4^{Me} Mp, 265–270°C dec. IR (CH_2Cl_2) ν_{co} 2036, 1930, 1923 c^{m-1}. ^{1}H NMR: (acetone-d_6, 293 K) 8.78 (d, *J* = 2.8 Hz, 1H, H_5pz), 8.06 (d, *J* = 2.8 Hz, 1H, H_5pz), 8.00 (part of AB d, J_{app} = 8.4 Hz, 1H, Ar), 7.72 (s, 1H, Ar), 7.66 (part of AB, d, J_{app} = 8.4, 2.1, 1 Hz, 1H, Ar), 7.57 (s, 1H, Ar), 7.04 (part of AB d, J_{app} = 8.4 Hz, 1H, Ar), 7.01 (d, *J* = 2.8 Hz, 1H, H4pz), 6.82 (part of AB d, J_{app} = 8.4 Hz, 1H, Ar), 6.33 (d, *J* = 2.8 Hz, 1H, H_4pz), 3.76 (s, 3H, NCH_3), 2.92 (s, 3H, CH_3), 2.53 (s, 3H, CH_3), 2.28 (s, 3H, CH_3), 2.06 (s, 3H, CH_3). UV-VIS λ_{max}, nm (ε, $M^{-1}c^{m-1}$), CD_2Cl_2: 242 (52,000), 289sh (13,000), 368 (1,300).

4^{iPr}.Mp, 260–265°C dec. IR(CH_2Cl_2) ν_{co} 2033, 1927, 1915 c^{m-1}. ^{1}H NMR: (acetone-d_6, 293 K) 8.79 (d, *J* = 3.0 Hz, 1H, H_5pz), 8.12 (d, *J* = 3.0 Hz, 1H, H5pz), 8.00 (part of AB d, J_{app} = 8.4 Hz, 1H, Ar), 7.71 (s, 1H, Ar), 7.66 (part of AB, d, J_{app} = 8.4, 2.1, 1 Hz, 1H, Ar), 7.53 (s, 1H, Ar), 7.17 (d, J = 2.8 Hz, 1H, H_4pz), 7.05 (part of AB d, J_{app} = 8.4 Hz, 1H, Ar), 6.82 (part of AB d, J_{app} = 8.4 Hz, 1H, Ar), 6.49 (d, *J* = 2.8 Hz, 1H, H_4pz), 3.93 (sept, *J* = 7 Hz, 1H, Me_2CH), 3.75 (s, 3H, NCH_3), 2.91 (sept, *J* = 7 Hz, 1H, Me_2CH), 2.54 (s, 3H, $ArCH_3$), 2.28 (s, 3H, $ArCH_3$), 1.57 (d, *J* = 7 Hz, 3H, iPrCH_3), 1.49 (d, *J* = 7 Hz, 3H, iPrCH_3), 1.22 (d, *J* = 7 Hz, 3H, iPrCH_3), 0.81 (d, *J* = 7 Hz, 3H, iPrCH_3). UV-VIS λ_{max}, nm (ε, $M^{-1}cm^{-1}$), CD_2Cl_2: 242 (50,000), 293sh (9,000), 367 (400).

Dalton Transactions, Vol. 40, No. 35 (September 2011): pg. 8776-8787. DOI.

Table 3 Crystal and structure refinement data for $H(L^{Me})$, 1^{Me}·acetone, 2^{Me}, and 3^{Me}

	$H(L^{Me})$	1^{Me}·acetone	2^{Me}	3^{Me}
Empirical Formula	$C_{22}H_{23}N_5$	$C_{26}H_{29}BrN_5O_4Re$	$C_{25}H_{23}F_6N_5O_3PRe$	$C_{22}H_{22}N_5O_3Re$
Formula Weight	357.45	765.67	772.65	626.68
T/K	100(2)	100(2)	100(2)	100(2)
Crystal Size/mm	0.43 × 0.18 × 0.12	0.24 × 0.13 × 0.05	0.26 × 0.21 × 0.10	0.24 × 0.14 × 0.06
Crystal System	Orthorhombic	Triclinic	Triclinic	Monoclinic
Space Group	*Pbcn*	*P*$\bar{1}$	*P*$\bar{1}$	*C*2/*c*
a/Å	14.6980(3)	10.8094(2)	8.63640(10)	30.8054(4)
b/Å	7.7505(2)	10.9596(2)	9.66670(10)	11.4882(2)
c/Å	33.6382(8)	13.4496(2)	16.7540(2)	13.4222(2)
α (°)	90	84.7710(10)	78.9030(10)	90
β (°)	90	85.0860(10)	82.4590(10)	94.7730(10)
γ (°)	90	60.9190(10)	78.8010(10)	90
V/Å^3	3831.96(16)	1385.10(4)	1340.01(3)	4733.63(12)
Z	8	2	2	8
d_c/g cm^{-3}	1.239	1.836	1.915	1.759
λ(Cu-Kα)/Å	1.54178	1.54178	1.54178	1.54178
μ/mm^{-1}	0.597	10.630	10.165	10.350
Abs. Correction	multi-scan	numerical	numerical	numerical
F(000)	1520	748	752	2448
θ range (°)	2.63 to 67.97	3.30 to 67.89	2.70 to 67.70	2.88 to 68.02
Reflections collected	32005	11557	11073	19490
Reflections unique	3444	4733	4556	4198
R_{int}	0.0306	0.0150	0.0168	0.0204
T_{min}/T_{max}	0.7835/0.9318	0.1847/0.6185	0.1775/0.4297	0.1902/0.5756
Data/restraints/parameters	3444/0/253	4046/0/363	4556/0/381	4198/0/311
GOF(F_2)	1.020	1.001	1.007	0.993
R indices[$I > 2\sigma(I)$][a] (all data)	0.0382 (0.0432)	0.0172 (0.0173)	0.0188 (0.0194)	0.0245 (0.0285)
wR indices (all data)[b]	0.0988 (0.1024)	0.0446 (0.0447)	0.0474 (0.0478)	0.0679 (0.0702)
Residuals/e A^{-3}	0.237/−0.158	0.613/−0.548	0.714/−0.646	0.815/−0.565

[a] $R_1 = \Sigma||F_o| - |F_c||/\Sigma|F_o|$. [b] $wR_2 = \{\Sigma[w(F_o^2 - F_c^2)^2]/\Sigma[w(F_o^2)^2]\}^{1/2}$.

Table 4 Crystal and structure refinement data for 1^{iPr}, 2^{iPr}, 3^{iPr} and 4^{iPr}·2CH_2Cl_2

	1^{iPr}	2^{iPr}	3^{iPr}	4^{iPr}·2CH_2Cl_2
Empirical Formula	$C_{26}H_{31}BrN_5O_3Re$	$C_{25}H_{31}F_6N_5O_3PRe$	$C_{25}H_{30}N_5O_3Re$	$C_{27}H_{37}Cl_4IN_5O_3Re$
Formula Weight	763.70	828.76	682.78	994.57
T/K	100(2)	100(2)	100(2)	100(2)
Crystal Size	0.15 × 0.14 × 0.10	0.23 × 0.10 × 0.06	0.28 × 0.16 × 0.06	0.33 × 0.07 × 0.04
Crystal System	Orthorhombic	Monoclinic	Monoclinic	Triclinic
Space Group	$P2_12_12_1$	$P2_1/c$	$P2_1/c$	*P*$\bar{1}$
a/Å	13.1679(2)	9.49510(10)	15.7528(2)	10.9417(3)
b/Å	13.4486(2)	14.9707(2)	13.73050(10)	12.1830(2)
c/Å	16.2017(2)	22.1068(3)	13.76030(10)	15.7817(3)
α (°)	90	90	90	73.5426(18)
β (°)	90	100.1190(10)	114.662(1)	85.7981(19)
γ (°)	90	90	90	65.475(2)
V/Å^3	2869.16(7)	3093.56(7)	2704.79(4)	1833.16(7)
Z	4	4	4	2
d_c/g cm^{-3}	1.768	1.779	1.677	1.802
λ(Cu or Mo-Kα), Å	1.54178	1.54178	1.54178	0.7107
μ/mm^{-1}	10.234	8.854	9.110	4.487
Abs. Correction	numerical	numerical	numerical	numerical
F(000)	1496	1632	1352	968
θ range (°)	4.27 to 68.17	3.58 to 67.61	3.09 to 68.20	3.30 to 32.72
Reflections collected	23851	25065	22830	59279
Reflections unique	5079	5429	4810	12747
R_{int}	0.0216	0.0223	0.0173	0.0330
T_{min}/T_{max}	0.3090/0.4276	0.2353/0.6187	0.1847/0.6109	0.349/0.866
Data/restraints/parameters	5079/0/362	5429/0/416	4810/0/350	12747/0/422
GOF(F_2)	0.992	0.992	0.999	1.040
R indices[$I > 2\sigma(I)$][a] (all data)	0.0168 (0.0170)	0.0219 (0.0252)	0.0178 (0.0182)	0.0191 (0.0241)
wR indices (all data)[b]	0.0428 (0.0429)	0.0541 (0.0554)	0.0462 (0.0465)	0.0456 (0.0463)
Residuals/e A^{-3}	0.642/−0.458	0.682/−0.628	0.578/−0.606	1.006/−0.896

[a] $R_1 = \Sigma||F_o| - |F_c||/\Sigma|F_o|$. [b] $wR_2 = \{\Sigma[w(F_o^2 - F_c^2)^2]/\Sigma[w(F_o^2)^2]\}^{1/2}$.

Crystallographic Structure Determinations

X-ray intensity data from a colorless prism of H(**L^{Me}**), colorless block of each $ReBr(CO)_3$[H(**L^{Me}**)]·acetone (**1^{Me}**·acetone), $ReBr(CO)_3$[H(**L^{iPr}**)] (**1^{iPr}**), {Re(CO)^3[H(**L^{Me}**)]}(PF6), (**2^{Me}**),

Dalton Transactions, Vol. 40, No. 35 (September 2011): pg. 8776-8787. DOI.

and{$Re(CO)_3[H(\mathbf{L^{iPr}})]$}(PF6), ($\mathbf{2^{iPr}}$), of a yellow block of $Re(CO)_3(\mathbf{L^{Me}})$, ($\mathbf{3^{Me}}$), and of a pale yellow block of $Re(CO)_3(\mathbf{L^{iPr}})$, ($\mathbf{3^{iPr}}$), were measured at 100(2) K with a Bruker AXS 3-circle diffractometer equipped with a SMART2[19] CCD detector using Cu(Kα) radiation. X-ray intensity data from a colorless needle of {$Re(CO)_3[Me(\mathbf{L^{iPr}})]$}(I)·$2CH_2Cl_2$, ($\mathbf{4^{iPr}}$·$2CH_2Cl_2$) were measured at 100(2) K with an Oxford Diffraction Ltd. Supernova diffractometer equipped with a 135 mm Atlas CCD detector using Cu(Ka) (or Mo(Ka) for $\mathbf{4^{iPr}}$·$2CH_2Cl_2$) radiation. Raw data frame integration and Lp corrections were performed with SAINT+.[20] Final unit cell parameters were determined by least-squares refinement of 5019, and 9735 reflections from the data sets of $\mathbf{1^{Me}}$·acetone, and $\mathbf{1^{iPr}}$, respectively, of 8854, and 7055 reflections from the data sets of $\mathbf{2^{Me}}$ and $\mathbf{2^{iPr}}$ respectively, and of 8940, and 8003 reflections from the data sets of $\mathbf{3^{Me}}$ and $\mathbf{3^{iPr}}$, respectively, and of 38198 reflections from the data set of $\mathbf{4^{iPr}}$ with I > 2s(I) for each. Analysis of the data showed negligible crystal decay during collection in each case. Direct methods structure solutions, difference Fourier calculations and full-matrix least-squares refinements against F2 were performed with SHELXTL.[21] Numerical absorption corrections based on the real shape of the crystals for the compounds were applied with SADABS.[20] All non-hydrogen atoms were refined with anisotropic displacement parameters. Hydrogen atoms were placed in geometrically idealized positions and included as riding atoms, except where noted below. The X-ray crystallographic parameters and further details of data collection and structure refinements are presented in Tables 3 and 4.

Acknowledgements

JRG thanks Marquette University and the NSF (CHE-0848515) for financial support. Support for ESR spectral studies (Grant NIH-RR001980) is also gratefully acknowledged.

Notes and references

1. O. V.Ozerov, The Chemistry of Pincer Compounds, D.Morales-Morales and C. M. Jensen, Eds; Elsevier: New York, Chapter 13, 2007.
2. A. T. Radosevich, J. G. Melnick, S. A. Stoian, D. Bacciu, C.-H. Chen, B. M. Foxman, O. V. Ozerov and D. G. Nocera, Inorg. Chem., 2009, **48**, 9214; J. I. von der Vlugt and J. N. H. Reek, Angew. Chem., Int. Ed.,

2009, **48**, 8832 and references; A. I. Nguyen, K. J. Blackmore, S. M. Carter, R. A. Zarkesh and A. F. Heyduk, J. Am. Chem. Soc., 2009, 131, 3307 and references; D. Adhikari, S.Mossin, F. Basuli, J. C. Huffman, R. K. Szilagyi, K.Mayer and D. J.Mindiola, J. Am. Chem. Soc., 2008, 130, 3676; S. B. Harkins and J. C. Peters, Inorg. Chem., 2006, **45**, 4316; S. B. Harkins and J. C. Peters, J. Am. Chem. Soc., 2005, **127**, 2030; S. B. Harkins and J. C. Peters, J. Am. Chem. Soc., 2004, **126**, 2885.

3. S. Wanniarachchi, B. J. Liddle, J. Toussaint, S.V. Lindeman, B. Bennett; and J. R. Gardinier, Dalton Trans., 2010, **39**, 3167.
4. B. J. Liddle, R. M. Silva, T. J. Morin, F. P. Macedo, R. Shukla, S. V. Lindeman and J. R. Gardinier, J. Org. Chem., 2007, 72, 5637; M. Taillefer, N. Xia and A. Ouali, Angew. Chem., Int. Ed., 2007, **46**, 934 and references; J. C. Antilla, J.M. Baskin, T. E. Barder and S. L. Buchwald, J. Org. Chem., 2004, **69**, 5578.
5. L. Fan, B. M. Foxman and O. V. Ozerov, Organometallics, 2004, 23, 326.
6. S. Trofimenko, J.C. Calabrese, P. J. Domaille and J. S. Thompson, Inorg. Chem., 1989, **28**, 1091.
7. K. Chadwick, R. J. Davey, R. G. Pritchard, C. A. Hunter and D. Musumeci, Cryst. Growth Des., 2009, **9**, 1990; V. Zanker, H. H. Mantsch; and E. Erhardt, Anales de Quimica, 1968, **64**, 659; M. A. Salimov and V.M. Tatevskii, Dokl. Akad. Nauk. SSSR, 1957, 112, 890.
8. R. C. Sharma and R. K. Parashar, J. Inorg. Biochem., 1987, **29**, 225; A. V. Savitskii and T. M. Kosareva, Dokl. Akad. Nauk SSSR, 1971, **197**, 359; J. S. Decker and H. Frye, Z. Naturforsch. Teil B, 1966, **21**, 527.
9. B. J. Liddle, S. Wanniarachchi, S. V. Lindeman and J. R. Gardinier, J. Organomet. Chem., 2010, 1, 695.
10. S. Alves, A. Paulo, J. D. G. Correia, Â. Domingos and I. Santos, J. Chem. Soc., Dalton Trans., 2002, 4714.
11. B. Machura, R. Kruszynski, M. Jaworska, P. Lodowski, R. Penczek and J. Kusz, Polyhedron, 2008, 27, 1767.
12. A. J. Parker, J. Chem. Soc., 1961, 1328.
13. The average Re–N bond distance of 2.223Å in **4^{iPr}** is similar to 2.219Å found in **2^{iPr}** where the Re–N_{Ar} bond (2.306 Å) is longer and the two Re–N_{pz} (2.177, 2.185 Å) are shorter for the former than in the latter. It is also noted that the amino nitrogen is more pyramidal for **4^{iPr}** than **2^{iPr}** as evident from the smaller sum of angles around nitrogen not involving the methyl (326° *versus* 333°) and larger perpendicular distance of nitrogen from the mean plane of rhenium and aryl carbon atoms to which nitrogen is bound (0.576Å *versus* 0.519Å). The small but increased ligand distortion in **4^{iPr}** versus **2^{iPr}** is also found from the tolyl-tolyl and average pz-tolyl dihedral angles (73° *versus* 70° and 40° versus 37°, respectively).

Dalton Transactions, Vol. 40, No. 35 (September 2011): pg. 8776-8787. DOI.

14. R. Rathore, C. L. Burns, M. I. Deselinescu, S. E. Denmark and T. Bui, Org. Synth., 2005, **82**, 1.
15 The difference in EPR signal line shapes between ($\mathbf{3}^{\mathbf{H+}}$) and ($\mathbf{3}^{\mathbf{Me+}}$) or ($\mathbf{3}^{\mathbf{iPr+}}$) can be attributed to a number of factors. First, the rhenium hyperfine coupling is smaller than the overall line width in the latter two cases causing alteration of the hyperfine pattern. The relative intensities of the four middle lines (line 4 > 3 > 5 > 2) in the latter two spectra may also arise due to genuine asymmetry of the complexes to give higher order effects. The possibility formultiple conformers (where each has a slightly different g-value) and any dynamic equilibria involving these species may also contribute. Incomplete motional averaging seems unlikely given the small size of the molecule.
16. D. Chong, D. R. Laws, A. Nafady, P. J. Costa, A. L. Rheingold, M. J. Calhorda and W. E. Geiger, J. Am. Chem. Soc., 2008, **130**, 2692; F. A. Cotton, K. R. Dunbar, L. R. Falvello and R. A.Walton, Inorg. Chem., 1985, **24**, 4180.
17. S. P. Schmidt,W. C. Trogler and F. Basolo, Inorg. Synth., 1990, **28**, 160.
18 I. Noviandri, K. N. Brown, D. S. Fleming, P. T. Gulyas, P. A. Lay, A. F. Masters and L. Phillips, J. Phys. Chem. B, 1999, 103, 6713.
19. SMART APEX2 Version 2.0-2 Bruker Analytical X-ray Systems, Inc., Madison, Wisconsin, USA, 2005.
20. SAINT+ Version 7.23a and SADABS Version 2.05 TWINABS Bruker Analytical X-ray Systems, Inc., Madison, Wisconsin, USA, 2007.
21. G. M. Sheldrick SHELXTL, Version 6.1Bruker Analytical X-ray Systems, Inc., Madison, Wisconsin, USA, 2000.

Dalton Transactions, Vol. 40, No. 35 (September 2011): pg. 8776-8787. DOI.